2017

Accuracy Assessment of 3D Point Clouds Generated by Photogrammetry From Different Distances

Zhongming An
Michigan Technological University, zan1@mtu.edu

ACCURACY ASSESSMENT OF 3D POINT CLOUDS GENERATED BY PHOTOGRAMMETRY FROM DIFFERENT DISTANCES

By
Zhongming An

A REPORT
Submitted in partial fulfillment of the requirements for the degree of
MASTER OF SCIENCE
In Integrated Geospatial Technology

MICHIGAN TECHNOLOGICAL UNIVERSITY
2017

This report has been approved in partial fulfillment of the requirements for the Degree of MASTER OF SCIENCE in Integrated Geospatial Technology.

School of Technology

Report Advisor:	*Dr. Yushin Ahn*
Committee Member:	*Dr. Eugene Levin*
Committee Member:	*Dr. Curtis Edson*
School Dean:	*Dr. James Frendewey*

Contents

List of Figures

List of Tables

Abstract

Photogrammetry is playing more important role in many industries today, and thanks to Structure-from-Motion, 3D point clouds and 3D meshes can be produced and be used as a resource for surveying and documentation.

In this project, the accuracies of Structure-from-Motion generated point clouds from pictures taken from different distances are assessed to determine if the distance has a significant impact on the accuracy and what kind of pattern the accuracies will show if there is any. Due to space limit, an improvised turntable was used in order to mimic the condition where camera moves around the object. Multiple images were collected from different distances and corresponding point clouds were generated using Agisoft Photoscan. Using the generated point clouds, accuracy assessment was able to be carried out.

During the analysis, other than the impact of distance, a slight impact of different colors was found first visually and then also analyzed with similar method.

Introduction

Photogrammetry is one of the many methods of obtaining accurate data, and thanks to those structure-from-motion algorithms, 3D point cloud and the 3D meshes of objects can be produced and thus, the application of photogrammetry has been a useful tool in many industries, including surveying, archaeology, entertainment, etc.

Many people have done a lot of research on the accuracy of photogrammetry and claim that photogrammetry is an accurate method to obtain field data. In 2014, team of Bolognesi surveyed the Delizia Estense del Verginese located in the province of Ferrara, Italy, and compared the photo-generated 3D point cloud to the points collected by total station and point cloud derived from terrestrial laser scanning, and eventually found "a good agreement between the point clouds of the castle derived from an integrated photogrammetric survey and from TLS and control points determined by total station". The team of Caroti (2015) surveyed San Miniato's church in Marcianella (Cascina, Pisa, Italy), and assessed the accuracy of the generated 3D point cloud and made a comparison with classic surveying method and laser scanning. They found that the number and distribution of ground control points affects the accuracy of the generated model. Team of Barrile used similar approach in 2015 to assess the accuracy and instead of 3D point cloud, they compared the generated 3D mesh and came to the conclusion that "low cost" photogrammetric method shows "a mean deviation of 2 centimeters and is very close to data obtained by laser scanning".

But will the distance affect the accuracy? Will the accuracy decrease with the increase of distance? Will the changes of accuracy follow a certain pattern that can be modeled and be used to predict accuracies according to the distance?

In this project, I will primarily try to find out how the accuracy will react to the change of distance and to determine if distance affects accuracy significantly.

Background

Photogrammetry

Definition of Photogrammetry

Photogrammetry is defined by the American Society for Photogrammetry and Remote Sensing (ASPRS) as the art, science and technology of obtaining reliable information about physical objects and environment through process of recording measuring, and interpreting photographic images and patterns of recorded radiant electromagnetic energy and other phenomena. (Wolf, et al., 2014)

There are two types of photogrammetry: metric photogrammetry and interpretive photogrammetry (Wolf, et al., 2014). The applications of these two types of photogrammetry cater to different requirements and thus produce different results.

Metric photogrammetry can provide precise relative positions and geometric information of objects and environment by making precise measurements on photographs. The major objective of interpretive photogrammetry, on the other hand, is to recognizing objects from photographs and determine the significance of these objects through carful and systematic analysis.

Applications of Photogrammetry

One major application, which also happens to be the oldest, is producing topographic maps (Wolf, et al., 2014, Kraus, 2004). This application of photogrammetry is still one of the most common activities.

Thanks to the digitization of photographs and the development of Structure from Motion (SfM) algorithms, orthophoto and Digital Elevation Model (DEM) can be produced. Instead of using lines and points to represent features in a planimetric map, an orthophoto, which is a photograph that is modified so that the scale is uniform throughout, showing objects in the true orthographic positions (Wolf, et al., 2014), uses images to represent those features and thus, is much easier for people to interpret (Wolf, et al., 2014). A DEM contains an array of points with X, Y and Z coordinates, which

provides numerical representation of the topolography in an area (Wolf, et al., 2014). Many other commonly used products, such as contours, cross sections, etc., can be produced using a DEM.

Photogrammetry has been an important tool in surveying industry for decades. Aerial photos can be used as rough base maps, which can help pinpoint locations if there are known points in the area. These photos can also be used as a reference for planning the fieldwork. Maps can be produced using aerial photos especially for those areas where it is difficult or impossible for surveyors to go in.

Other than surveying application, photogrammetry also plays important roles in architecture, archaeology, traffic management and accident investigation, etc. Nowadays, people can also easily turn photos into 3D models with free or low-cost software, which give many artist new ways of creating artworks. Photogrammetry is also playing more and more important part in the entertainment industry.

Brief History of Photogrammetry

Even though many concepts commonly used in photogrammetry existed long before the first photograph was developed in 1827 (Griggs, 2014, Wolf, et al., 2014), the practice of photogrammetry started after the practical method was developed. In 1849, the actual experiment in using photogrammetry for topographic mapping was commenced by the French Army Corps of Engineers. Kites and balloons were used at first to obtain aerial photos but the plan was abandoned due to technical difficulties. But the terrestrial photogrammetry in topographic mapping was quite successful (Wolf, et al., 2014).

The invention of plane gives photogrammetry a whole new platform, especially for military operations. Before this, technical issues limited photogrammetry to terrestrial platforms (Wolf, et al., 2014). During World War I, aerial photos were extensively used for reconnaissance purposes (Wolf, et al., 2014). During the period between World War I and World War II, aerial photogrammetry for topographic mapping was used as a tool to produce maps massively (Wolf, et al., 2014). During WWII, aerial photos

were extensively used in reconnaissance and map production (Wolf, et al., 2014). Figure 1 and 2 show examples of military application of aerial photos.

(a) (b)

Figure 1. Aerial photos taken before the Battle of Passchendaele (a) and after the battle (b) during WWI (Courtesy Daily Mail.com)

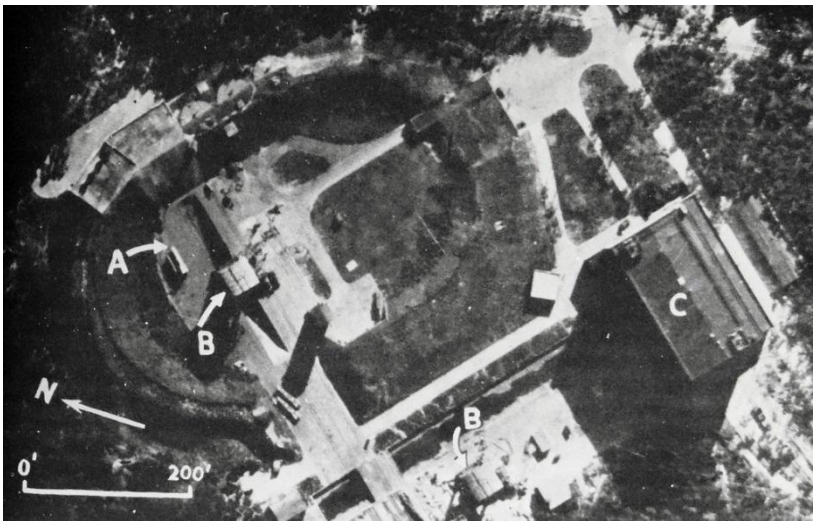

Figure 2. Aerial photo of a V2 launch site, Peenemunde, during WWII (Courtesy Wikipedia)

After WWII, with the appearance of new technologies and platforms, such as digitization of photographs and satellites, the application of photogrammetry greatly extended, and new products like orthophoto, DEM, 3D model, etc.

could be produced. Figure 3 shows the traditional orthophoto and generated true orthophoto produced using DEM, Digital Building Model (DBM), and images by Deng, et al., 2015.

(a) (b)

Figure 3. Traditional orthophoto (a) and generated true orthophoto (b) produced by Deng, et al., 2015

Camera Calibration

Generally, the process of photogrammetric survey follows the steps below:

1. Interior orientation: a process where the geometry of the projected rays is created to duplicate the geometry of the original photos.
2. Relative orientation: a process where the relative position between a pair of photos is recreated.
3. Absolute orientation: a process where the model is registered to a known reference system.

Cameras are carefully calibrated to determine precise and accurate values for the elements of interior orientation, which are calibrated focal length, symmetric radial lens distortion, decentering lens distortion, principal point location and fiducial mark coordinates (Wolf, et al., 2014).

To calibrate cameras, several models are developed. Brown developed a calibration model in 1971, where the coefficients of radial distortion and decentering distortion are defined. A 10-parameter model for digital camera self-calibration was developed by Fraser in 1997.

Nowadays, many digital cameras include distortion correction function, which means distortion of the photos taken by these cameras are corrected. But for cameras that can use different lenses, extra calibration for a specific lens is necessary. When using SfM software to produce 3D point clouds, the software can calibrate the camera automatically by accessing the metadata of the photos. One can also use a pre-calibrated file, which contains the elements of interior orientation.

One way to pre-calibrate the camera is using Agisoft Lens software. The software will display a checkerboard pattern on the screen and photos occupied only by the checkerboard from slightly different angles shall be taken. Using these photos, the software will calculate the focal length, coordinates of principal point and distortion parameters in the unit of pixel. All the information will eventually be stored in an xml file and can be used when producing point cloud. If a zoom lens is used, different focal lengths should be treated as independent lenses and calibrated separately (Agisoft Photoscan User Manual). Figure 4 shows the suggested way of taking photos to calibrate the camera.

(a) (b)

Figure 4. Incorrect way (a) and correct way (b) of taking photos for calibration suggested by Agisoft Lens Manual

Structure from Motion

Structure from Motion (SfM) is a newly developed low-cost photogrammetry and computer vision approach to obtaining high-resolution spatial data. SfM algorithm uses feature recognition algorithm to identify common features in

image pairs and calculate camera positions and poses and scene geometry automatically, eliminating the requirement to identify image control manually (Westoby, 2012).

The appearance of SfM greatly cut down the budget of 3D scanning projects. However, there are certain limitations to this method. One should avoid non-textured or self-resembling surface, shiny, highly reflective or transparent objects (Agisoft Photoscan User Manual; Schaich, 2013).

Shiny objects should be avoided but if the shiny object is the object of interest, one should try to shoot the object under a cloudy sky (Agisoft Photoscan User Manual). Transparent object should be avoided, but with proper coating, one still can get the desired result (Busby, 2016).

Taking Photos

If one wants to obtain good photo scanned 3D point cloud or 3D mesh, one should try to obtain photographs vertical to the surface of interest when the photos are taken. The developer of Agisoft photoscan provide several advices for how to obtain photos that can be used for the 3D point cloud generation. The figures below show the suggested scenarios of improper and proper methods of taking photos (Agisoft Photoscan User Manual).

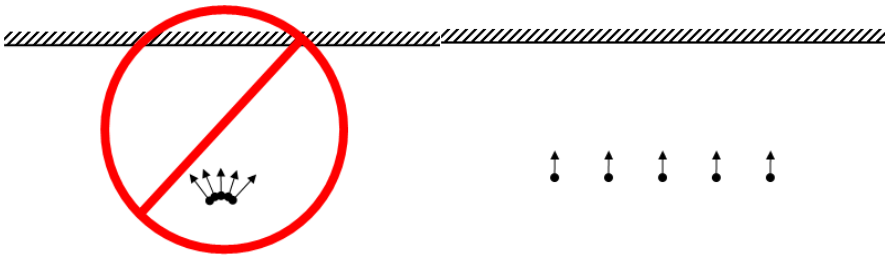

(a) (b)

Figure 5. Incorrect (a) and correct (b) ways of photo collection for facade

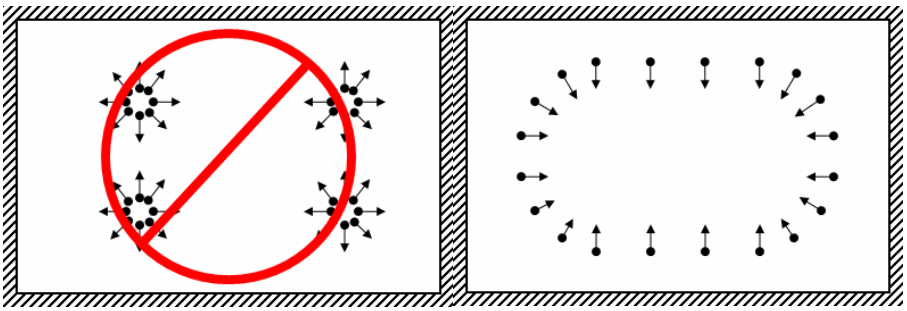

(a) (b)

Figure 6. Incorrect (a) and correct (b) ways of photo collection for interior

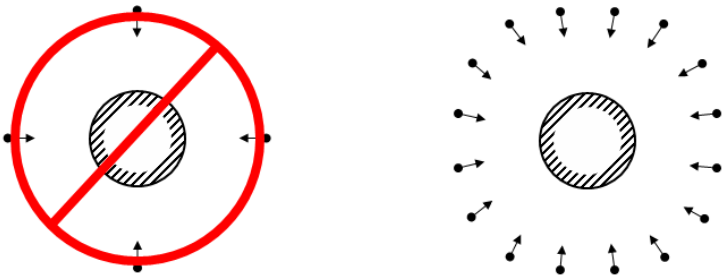

(a) (b)

Figure 7. Incorrect (a) and correct (b) ways of photo collection for isolated object

By taking photos in ways presented above, one is able to obtain mostly vertical photographs or nearly vertical photographs, which will provide information that is less distorted, but the photos do not have to be truly vertical to provide reasonably accurate information (Aniya, et al., 1986).

Methods

Many researchers have conducted accuracy assessments on photogrammetry and they claim that the method is accurate (Bolognesi, et al., 2014; Fonstad, et al., 2012), which is comparable to aerial LiDAR method (Fonstad, et al., 2012), and low-cost (Westoby, et al. 2012; Schaich, 2013). In their studies, both photos and spatial data are collected and after geo-referencing, some parameters are compared to determine the accuracy and precision of photogrammetry generated 3D point cloud (Bolognesi, et al., 2014, Caroti, et al., 2015, Fonstad, et al., 2012). In this project, I will use a similar approach, but to assess accuracies only of point clouds generated from photos taken from different distances.

Equipment

In this project, I used a Nikon D7000 DSLR primarily for the data collection. The aperture is set to f/22, which is the smallest for this camera and can largely neutralize the effect of depth of field, producing a sharper image (Mansurov, 2017).

Due to a lack of lighting, the shutter speed was set to 6 seconds in order to capture as much lighting information as needed. A tripod was used to stabilize the camera since a longer exposure was used. The lens is a Nikkor 18-105 mm zoom lens. In this case, only the focal length of 18 mm and 105 mm was used because those lie between the two settings are less stable and more vulnerable to human errors.

I also used some improvised devices in this project. A turntable was made from a dumbbell and some cardboard boxes. A cone cap was 3D printed and attached to the bottom of the tripod so that the camera position could be pinpointed. Figure 8 (a) and (b) shows the improvised devices.

Target object

In this project, the target object is a cardboard box with multiple markers on it. One of the planes of the box is the major subject of analysis. Since the box is vulnerable to external forces, movement of the box was carried out with extreme caution. Figure 9 shows the cardboard box used in this project. The side with coded targets on is the major area that this project is focused on.

(a) (b)

Figure 8. Improvised turntable (a) and cone cap (b)

Figure 9. Target object

Data Collection

The process of data collection consists of two major parts: image collection and spatial data collection.

Image collection

When taking pictures of an object, it is recommended by Agisoft Photoscan User Manual that the camera moves around the object, so that one can capture different perspectives of the object and create a 3D point cloud. When space is limited, one can use a turntable, but in this case, masks must be created for each photo and pixels beyond the mask be ignored. Thus the situation where the camera moves around the object is imitated. Figure 10 shows pictures of one of the tests, where the photos were taken with the camera of a Nexus 5 cellphone. The camera was pre-calibrated.

The camera was pre-calibrated for both focal lengths using Agisoft Lens, a commercial software. The software primarily uses Brown's calibration model (Agisoft photoscan user manual). Table 1 shows the calibrated parameters in the unit of pixel for both focal lengths.

Table 1. Calibration parameters for 18mm and 105 mm focal length

	18 mm	105 mm
Height	3264	3264
Width	4928	4928
f_x	3658.9569817740216	18198.789593456106
f_y	3659.4597328344285	18213.122398779513
C_x	2486.1276368706272	2409.7625381549251
C_y	1661.1283877930912	1672.8309988469737
K_1	-0.063880959996787168	0.11484825557318452
K_2	0.099974304038134926	2.6938376961411938
K_3	-0.21487481112925083	8.2863883354860235
Skew	1.4903332986136344	-9.0715811379925597

P_1	-0.00011805891865988113	-0.0014981131813859394
P_2	0.00080504445696621366	0.00020818800918475381

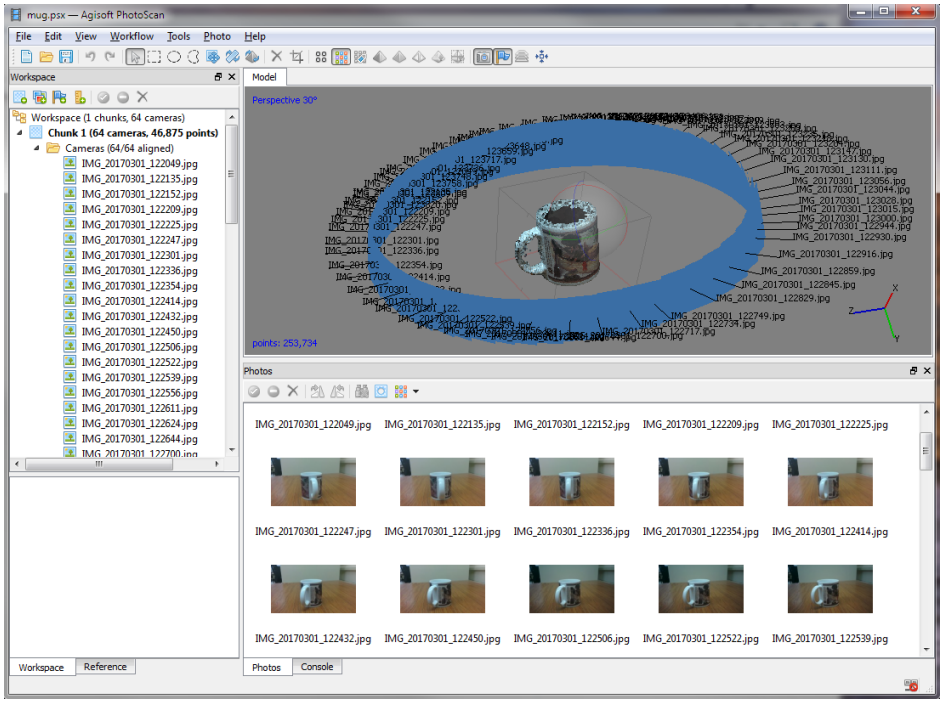

Figure 10. Turntable method demonstration

In this project, because of the limitation of space, an improvised turntable was used. In this case, the camera stays stationary and the object placed on the turntable rotates. After collecting photos, all photos were masked in Agisoft Photoscan, a commercial software, mimicking the condition where the camera moves around the object. The software automatically generated all the masks first but it still required some manual modification to get the best result.

For the focal length of 18mm, 10 sets of images were taken from 10 different distances, from 2 meters to 20 meters with an interval of 2 meters, and each set contained 16 images of the desired face of the box. A compass was used to determine the rotation interval angle, which is 6 degrees. This interval

angle ccould ensure an sufficient overlap, which was at least about 60%, to produce point clouds.

For the focal length of 105 mm, 10 sets of images also were taken under the same condition, but when the camera was at the distance of 2 meters, the field of view did not cover the whole target, and thus an extra set of 16 images were taken to cover the full area of interest. Figure 11 is the visual presentation of the image collection process.

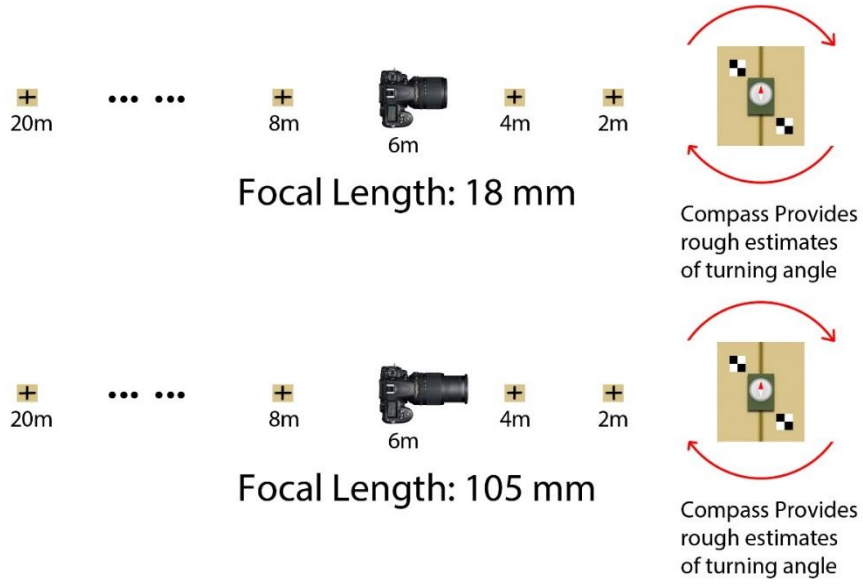

Figure 11. Image collection illustration

Spatial Data Collection

In this project, the reference system used is a local coordinate system defined by the author. In this system, the original point (0, 0, 0) is defined as the location of the first station, and the azimuth 0 is defined as an approximate direction of north.

The collection site was an office. Six checkerboard targets were placed on the walls, which was used to calculate the position of the second station, and the target object sit still in the room. A total station was used and two stations were setup to collect the coordinates of targets placed on the

cardboard box. Table 2 shows the collected coordinates in the unit of meter. Figure 12 and 13 show the collected points displayed in ArcGIS and the site setup.

Table 2. Coordinates of collected points

Point name	X/m	Y/m	Z/m	Description
s1	0	0	0	First station
cp001	1.467	-1.289	1.312	Checkerboard wall target
cp002	2.695	1.245	1.67	Checkerboard wall target
cp003	-2.496	1.746	1.65	Checkerboard wall target
cp004	-6.38	2.266	1.745	Checkerboard wall target
cp005	-6.789	-0.111	1.833	Checkerboard wall target
cp006	-2.712	-0.794	1.881	Checkerboard wall target
cpb001	-2.08	0.378	1.115	Checkerboard wall target
cpb002	-2.383	0.131	0.964	Checkerboard wall target
cpb007	-2.166	0.582	1.005	Checkerboard wall target
cpb008	-2.16	0.438	1.176	Checkerboard wall target
cpb009	-2.528	0.351	1.177	Checkerboard wall target
chp01	-2.247	0.241	1.012	Checkerboard wall target
chp02	-2.373	0.137	1.095	Checkerboard wall target
chp03	-2.107	0.358	0.892	Checkerboard wall target
s2	-4.506	0.761	-0.013	Second station, calculated by resection
cpb003	-2.508	0.186	1.04	Checkerboard box target

cpb004	-2.594	0.428	0.926	Checkerboard box target
cpb005	-2.457	0.541	1.062	Checkerboard box target
cpb006	-2.348	0.631	0.954	Checkerboard box target

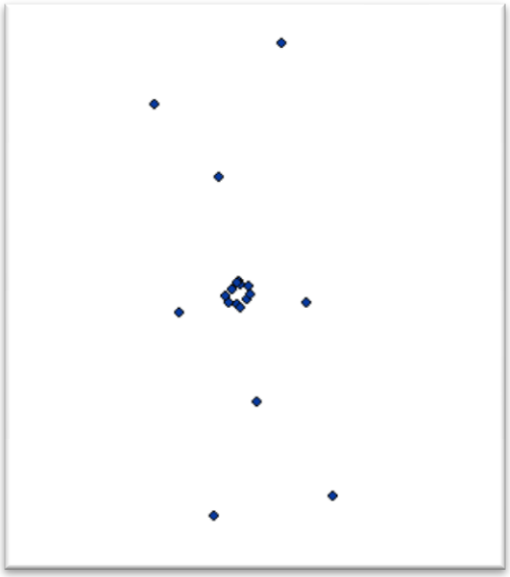

Figure 12. Collected points displayed in ArcGIS

(a) (b)

Figure 13. View from station 1 (a) and from station 2 (b)

After the photos were processed and the point clouds produced, an area of interest was selected and the point clouds were exported and imported to MATLAB for analysis to determine if distances have significant impact on the accuracies of the point clouds.

Analysis and Results

During the image collection, 352 images were acquired, including 160 images for the focal length of 18mm and 192 images for the focal length of 105mm. At the distance of 2 meters, the field of view of 105 mm was not able to cover the whole area of interest, and thus two extra sets of photos, containing 32 photos, were taken to cover all the area of interest.

Workflow of Generating Point Cloud Using Agisoft Photoscan

I took all the photos in the form of RAW images, which are in the format of NEF files, and converted the NEF files into DNG files using Adobe DNG converter, a free software. Then all the DNG files are converted into TIFF files without compression using Adobe Photoshop, a commercial software. I did not make any changes to the images in Photoshop, except that the white balance was adjusted in order to get a more natural visual effect. Finally I imported the TIFF files into Agisoft Photoscan and produced different sets of point clouds using exactly the same setting.

In this project, four coded targets were placed onto the surface of the box, which were able to be identified and marked by Agisoft Photoscan. The software detected the coded targets and then used them in the bundle adjustment process. After a preliminary bundle adjustment, the software was also able to detect the checkerboard targets. After the checkerboard targets are detected, I applied bundle adjustment the second time or even the third time so that a better registration among the photos can be achieved. Then the dense point cloud can be produced and all the markers that are surveyed with the total station are detected and renamed properly. Finally, I imported the coordinates surveyed using total station and as long as the name of a marker is identical to a surveyed point, the software will automatically georeference the point cloud. Figure 14 shows the process of producing dense point cloud in Agisoft Photoscan.

The figure below shows the produced dense point cloud from photos taken from a distance of 2 meters.

Figure 14. Dense point cloud produced in Agisoft Photoscan

Impact of Distance

After georeferencing the point cloud, Photoscan will automatically produce a simple report on the errors in the unit of meter.

The anticipated result would be the indicators for precision and accuracy increase with the increase of distance, but the analysis gave me a different result from what I had expected.

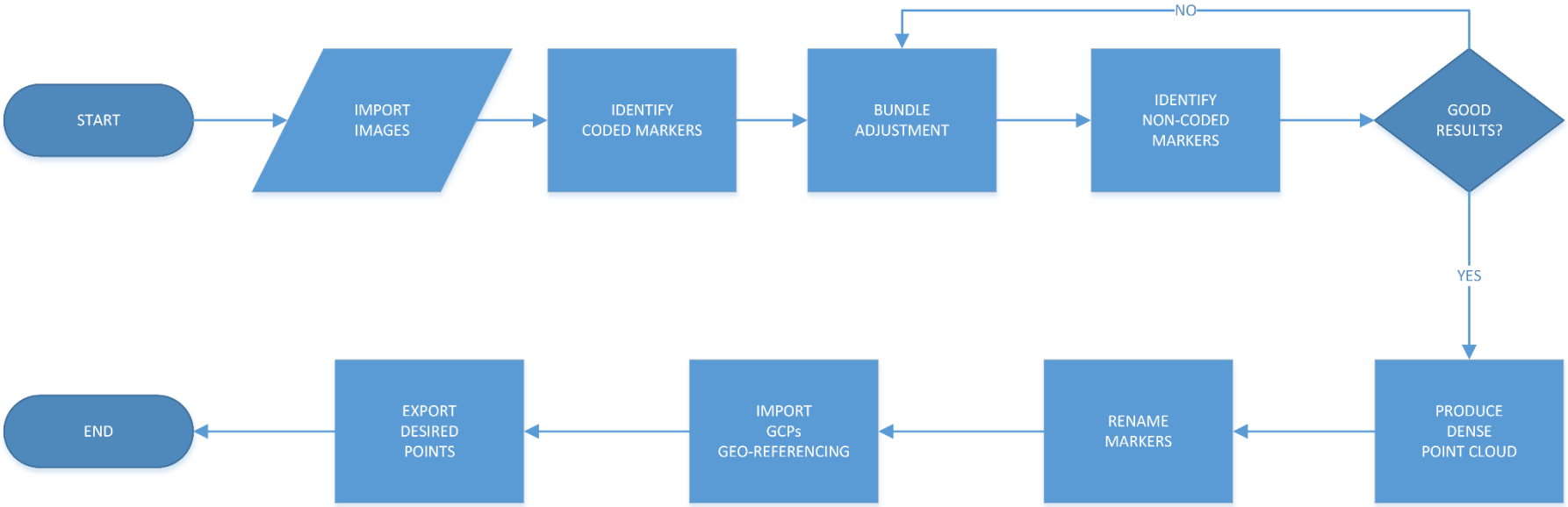

Figure 15. Process of producing dense point cloud

For the focal length of 18 mm, among the 10 sets of collected images, only the first set, which were taken from a distance of 2 meters were able to produce visually usable dense point cloud. For the rest of the images, some sparse point clouds were able to be produced but dense point clouds were not able to be produced. With the increase of the distance, it is also getting more difficult for the sparse point cloud to be produced, even with the markers placed on the box.

For the focal length of 105 mm, all of the images were successfully processed and dense point clouds were produced. With the increase of the distance, the number of points decreased in the condition where the same amount of photos were taken. Table 3 shows the number of tie points of the generated point clouds only using the focal length 105 mm. Most of the photos for 18 mm were even not able to produce sparse clouds, and thus, the project's focus was on 105 mm.

Table 3. Number of tie points of the point clouds

Focal length, distance	Photos	Number of tie points
105mm, 2m	48	44107
105mm, 4m	16	35880
105mm, 6m	16	17340
105mm, 8m	16	9360
105mm, 10m	16	6065
105mm, 12m	16	3639
105mm, 14m	16	2590
105mm, 16m	16	1805
105mm, 18m	16	1364
105mm, 20m	16	1025

According to the simple report provided by Photoscan on errors, there were fluctuations but the errors were generally stable. Table 4 shows the errors in the unit of meter in the report by Photoscan.

Table 4. Error Report by Photoscan

	chp01	chp02	chp03	cpb001	cpb001	Total
105mm,2m	0.001360	0.000134	0.000676	0.000591	0.000693	0.000794
105mm,4m	0.001294	0.000181	0.000728	0.000602	0.000714	0.000789
105mm,6m	0.001357	0.000153	0.000648	0.000599	0.000705	0.000793
105mm,8m	0.000907	0.000441	0.000374	0.000364	0.000596	0.000574
105mm,10m	0.001253	0.002221	0.004101	0.003775	0.002336	0.002933
105mm,12m	0.001360	0.000138	0.000666	0.000580	0.000686	0.000790
105mm,14m	0.001108	0.000319	0.000717	0.000552	0.000679	0.000722
105mm,16m	0.001196	0.000234	0.000676	0.000603	0.000655	0.000740
105mm,18m	0.001004	0.000642	0.000119	0.000455	0.000736	0.000661
105mm,20m	0.00154	0.000422	0.001205	0.000997	0.000889	0.001076

During the process, the bundle adjustment of Agisoft Photoscan turned out to be rather unstable, especially for pictures taken from a longer distance. In order to obtain a usable cloud, the procedure had to be done multiple times even with the same settings and makers. Figure 16 shows some different results of bundle adjustment.

I then manually cleaned the point clouds to remove obvious outliers and unnecessary points, and most of the front plane was selected from one of the clouds as the area of interest (AOI). The cleaned point clouds were then

exported as .ply files, which contain the coordinate information, normal, and RGB values of the points.

In MatLab, the AOI was used as a template so that when processing other clouds, the points participating in the analysis were from the same area. Figure 17 shows the AOI displayed by MatLab.

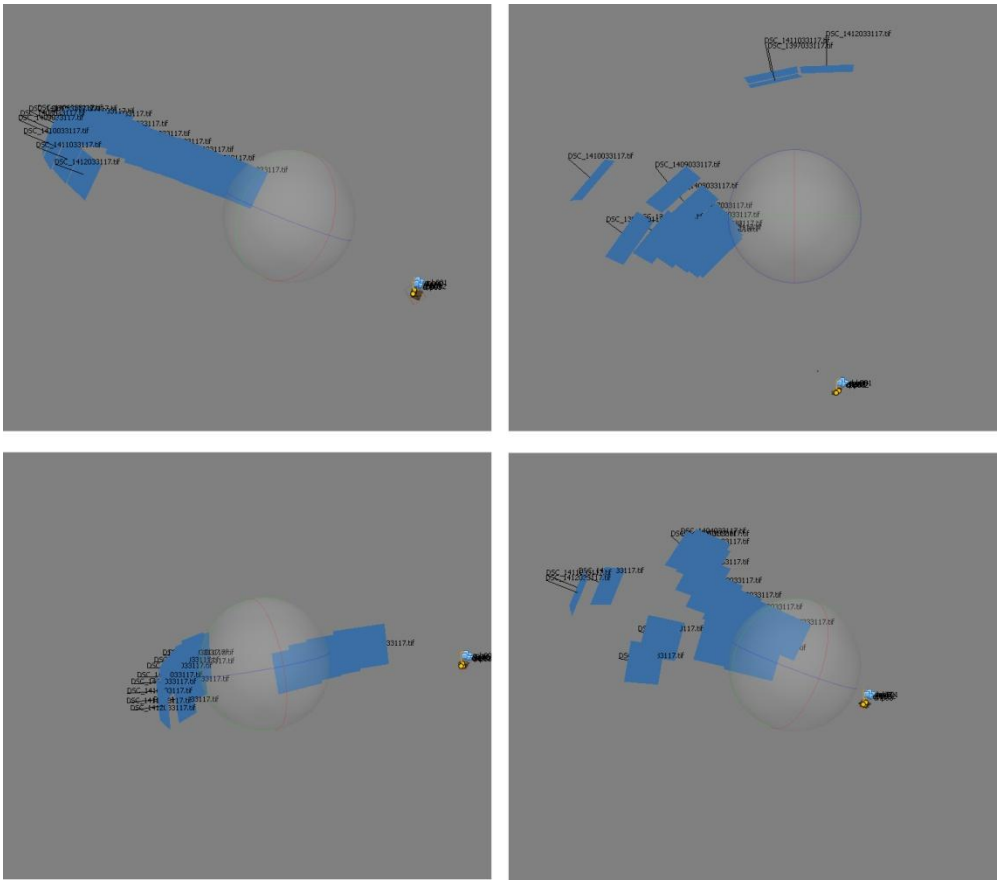

Figure 16. Different results from bundle adjustment

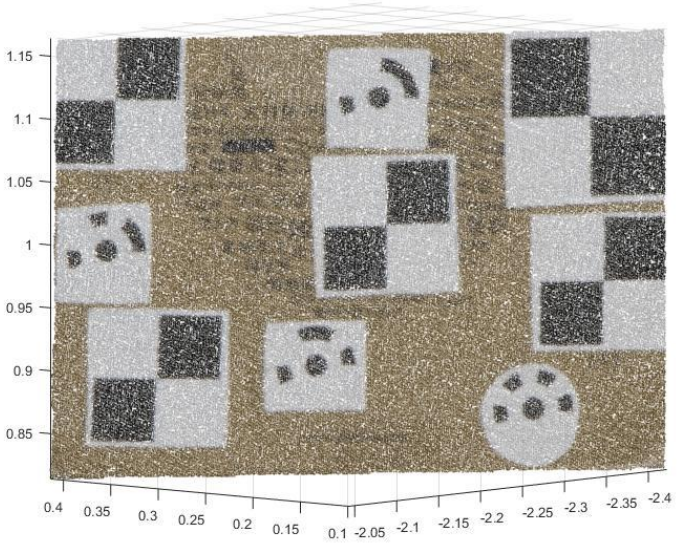

Figure 17. AOI displayed in MatLab

Code was used to extract points from the AOI, to fit planes and to calculate standard deviations in order to assess the accuracies of the clouds. In this case, the focal length of 105mm was assessed since the focal length of 18mm only produced one usable dense point cloud. The standard deviation, which is the deviation from the planes fitted from the point cloud, and the root mean square error (RMSE), which is the deviation from the plane fitted from points collected by the total station, were used to assess the accuracies for the clouds. Table 5, Table 6 and Figure 18 shows the standard deviations and the RMSEs of the point clouds in the unit of meter.

Table 5. Standard deviations of the point clouds

Focal length, distance	Standard deviation
105mm, 2m	0.00047
105mm, 4m	0.00048
105mm, 6m	0.00047
105mm, 8m	0.00056

105mm, 10m	0.00055
105mm, 12m	0.00054
105mm, 14m	0.00059
105mm, 16m	0.00089
105mm, 18m	0.00076
105mm, 20m	0.00074

Table 6. Root Mean Square Errors of the point clouds

Focal length, distance	Standard deviation
105mm, 2m	0.0013
105mm, 4m	0.0013
105mm, 6m	0.0013
105mm, 8m	0.0014
105mm, 10m	0.0013
105mm, 12m	0.0014
105mm, 14m	0.0014
105mm, 16m	0.0016
105mm, 18m	0.0013
105mm, 20m	0.0015

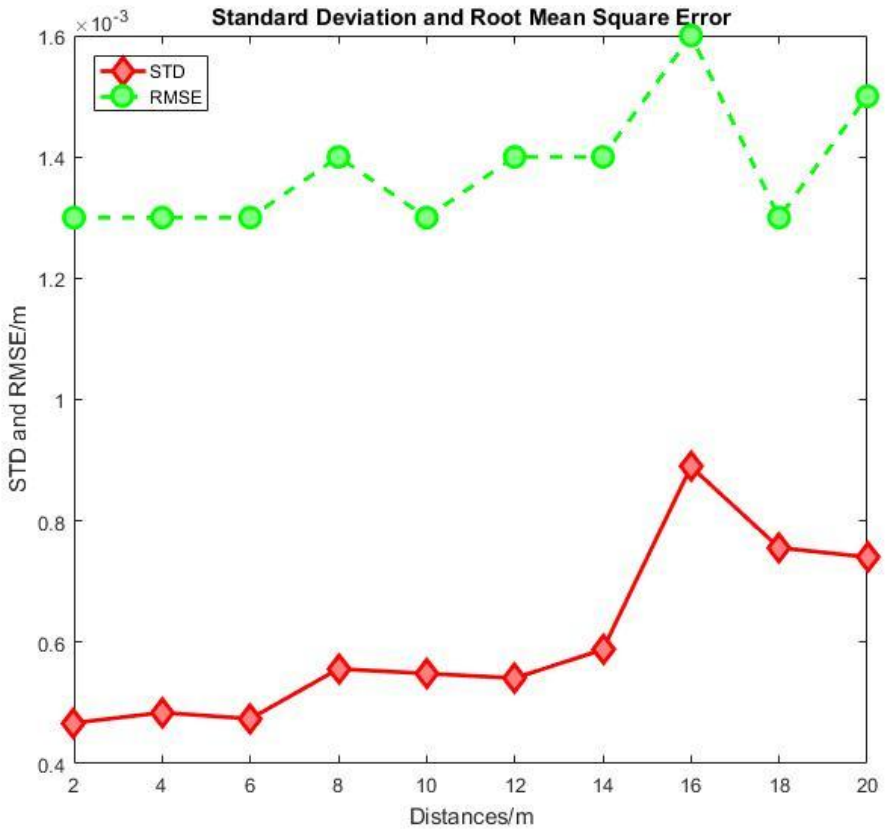

Figure 18. Standard deviations and RMSEs of the point clouds

From the figure, it is clear that for this camera and lens, within 20 meters, despite the fluctuation and the slight tendency of going up, the standard deviations and the RMSEs tend to be fairly small, which can be considered stable. That means within 20 meters, distance is not a significant factor that affects the accuracies of generated 3D point clouds. However, it cannot be determined that distances do not have a significant impact on the accuracy beyond 20 meters, and further data collection and analysis is required.

The Impact of Black and White

During the process of the set of images taken from 2 meters, using a focal length of 105 mm, the points of different colors seem to be on a different level, which are actually on the same plane. Figure 19 shows the visual difference of the impact of different color. From the figure, it can be seen

that the black area has much smoother surfaces than the white area and the boundaries of the two colors are recognizable.

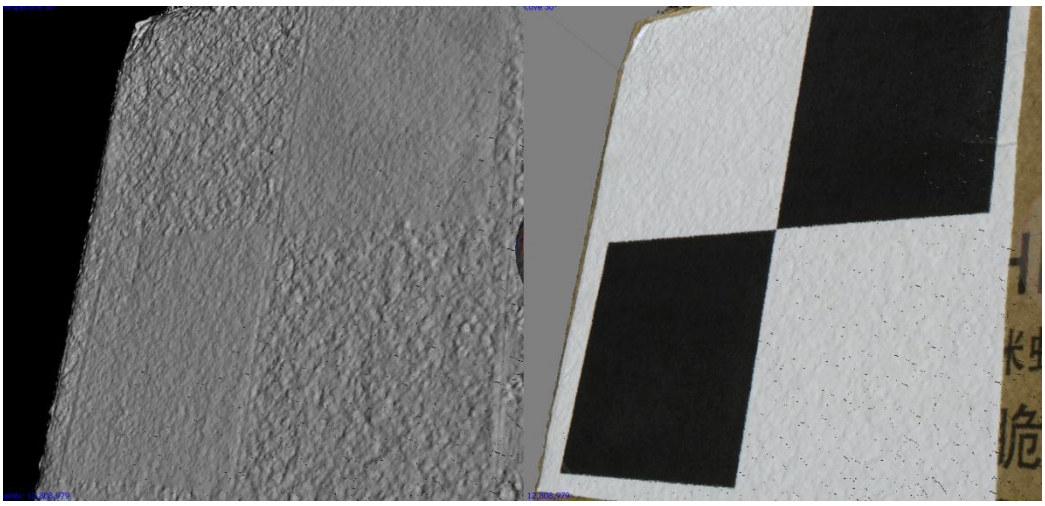

Figure 19. Visual Difference of color impact

In order to analyze the accuracy of areas of different colors, the white colored areas and black colored areas are extracted as the subjects. Figure 20 shows the extracted white areas and black areas displayed by MatLab.

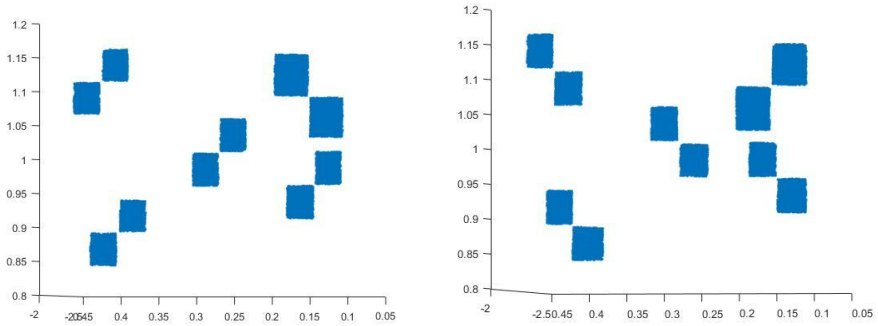

(a) (b)

Figure 20. Black areas (a) and white areas (b) displayed in MATLAB

In MatLab, same to the analysis on the whole plane, planes were fitted to the extracted points and the standard deviations and RMSEs were calculated to assess the accuracy of the points.

The tables and figure below show the calculated standard deviations and RMSEs for the point clouds in the unit of meter and the number of points of white area and black area participated in the processing.

Table 7. Standard deviations for white and black colored areas

Focal length, distance	WHITE	BLACK
105mm, 2m	0.00041	0.00030
105mm, 4m	0.00032	0.00028
105mm, 6m	0.00034	0.00029
105mm, 8m	0.00036	0.00036
105mm, 10m	0.00047	0.00034
105mm, 12m	0.00043	0.00038
105mm, 14m	0.00046	0.00046
105mm, 16m	0.00060	0.00047
105mm, 18m	0.00068	0.00083
105mm, 20m	0.00054	0.00054

Table 8. RMSEs for white and black colored areas

Focal length, distance	WHITE	BLACK
105mm, 2m	0.0014	0.0013
105mm, 4m	0.0014	0.0013
105mm, 6m	0.0015	0.0013
105mm, 8m	0.0014	0.0013

105mm, 10m	0.0014	0.0013
105mm, 12m	0.0015	0.0014
105mm, 14m	0.0015	0.0013
105mm, 16m	0.0016	0.0015
105mm, 18m	0.0015	0.0014
105mm, 20m	0.0016	0.0014

Table 9. Number of points participated in the analysis

Focal length, distance	WHITE	BLACK
105mm, 2m	831651	818826
105mm, 4m	212643	210610
105mm, 6m	99637	99140
105mm, 8m	56177	55985
105mm, 10m	36256	34978
105mm, 12m	26275	26006
105mm, 14m	19323	19152
105mm, 16m	14460	14371
105mm, 18m	11768	11484
105mm, 20m	9776	9612

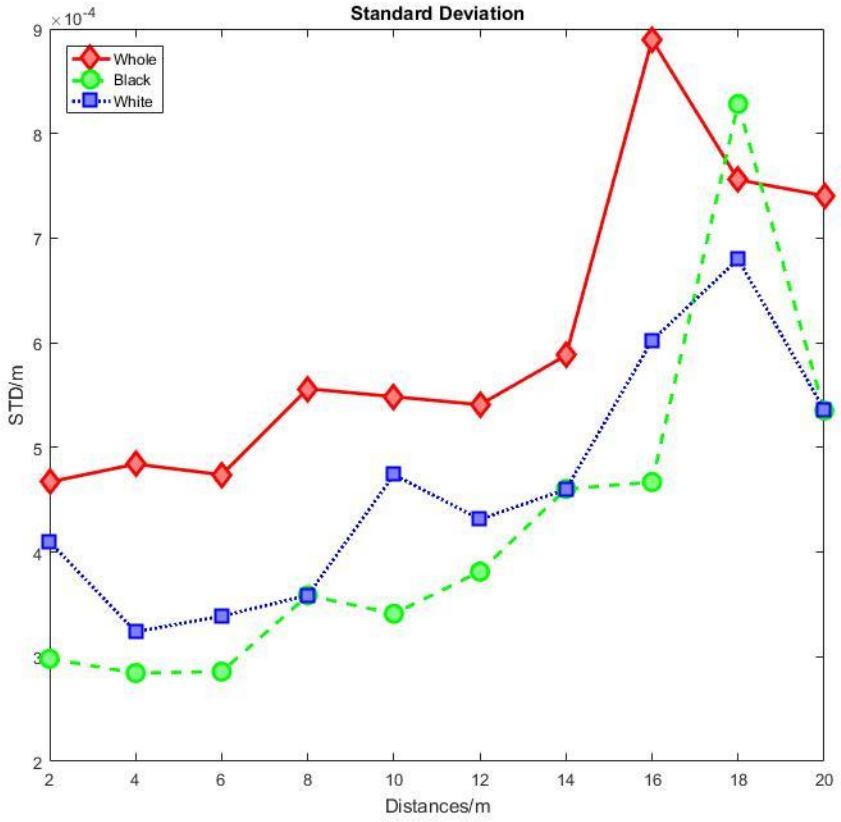

Figure 21. Standard deviations for both colors and the whole plane

Within 20 meters, points, generated by Agisoft Photoscan from photos taken by a Nikon D7000 with 105mm focal length, have, in general, consistent accuracies which are represented by their standard deviations and RMSEs. However, from the figure, it is obvious that the standard deviations and RMSEs of the black colored area are generally better than that of the white colored area, which possibly means that an object of a black color could produce a point cloud with better accuracy than an object with the same shape but a white color, but in this case, the differences are very small and thus it can be considered that there are no significant differences on accuracies between the two differently colored areas.

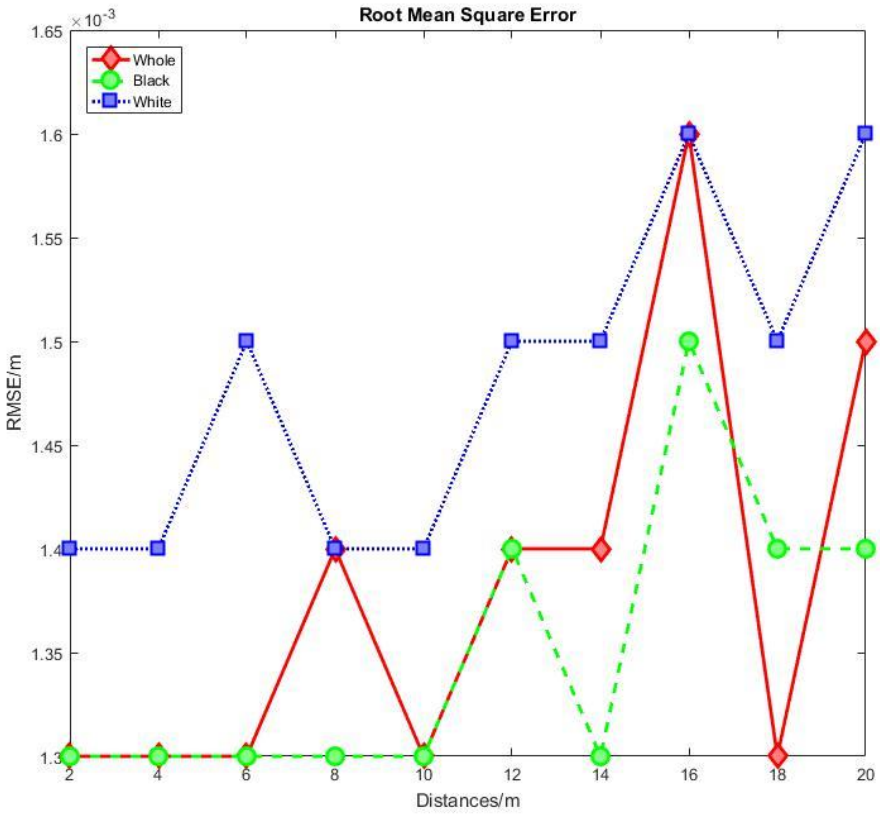

Figure 22. RMSEs for both colors and the whole plane

Advantages and Disadvantages of using a turntable

In this project, a turntable is used to help capture the photos. There are some advantages and disadvantages of using a turntable in this specific project.

Advantages:

- The camera is stationary, which means the operator does not have to move much, and it makes collecting photos in a limited space possible.
- The processing time decreases significantly since masks are used.
- Point cloud generated from a certain distance is good enough for future use.

Disadvantages:

- Masking the images takes some extra time and manual effort. Even though the masks applied to the images are not necessarily perfect matches to the silhouette of the object, some human effort is still required.
- The ability of bundle adjustment is limited. Since masks are used and the only area that is to be processed by the software is the object. With the increase of distance, this area becomes smaller and less capable of producing enough tie points.
- It still takes some time to process the data despite the fact that the process time has been decreased.

Future Work

This project demonstrates that distance does not significantly affect the accuracies of 3D point clouds generated from photos within 20 meters. With proper processing, photos taken within 20 meters are able to produce reasonably accurate 3D point cloud. It can be helpful during the planning process for a photogrammetric survey with a similar camera model knowing what accuracy to expect. It will be likely to become more helpful if further study can detect the pattern of accuracy changes with different distances that are over 20 meters.

In this project, because of the limits of space, the maximum analyzing distance is only 20 meters and thus all the results produced in this project only applies to situations where the photograph distances are within 20 meters. Even though it shows a slight trend where the accuracies will get worse with the increase of distance, it is not certain that it is going in that way. Thus, more data from longer distances will be possibly collected and analyzed to see the relationship between distances and accuracies for 3D point clouds and meshes produced using photogrammetry.

I will also spend more effort on the analysis of the impact of different colors. In this project, the targets are attached to the subject and thus the thickness of paper may have slightly affected the results.

Because it is a low-budget project, only one camera and one software are used but in the future, more camera models and lenses will possibly used and analyzed to see the accuracies of 3D point clouds produced from different cameras. I will also include more software to see the differences among different software.

Since the target is small and no check points are placed to assess the precision in this project, a bigger target like a building may be analyzed and check points will be placed to assess the precision as well.

Conclusion

In this project, photos of a cardboard box are taken from different distances and 3D point clouds are generated and geo-referenced to a local but the same coordinate system. By calculating and comparing the standard deviations and RMSEs of the point clouds, the conclusion can be drawn that within 20 meters, despite a slight ascending trend of both parameters, they are very small and can be considered stable, which means that distance is not a significant factor that affects the accuracy of a point cloud.

Black and white have slight impact on the accuracy of point clouds but the impact is very small and can be considered insignificant.

However, both conclusion only applies to situations where photos are taken within 20 meters. Further study on situations beyond 20 meters is required to determine the changing pattern of accuracy.

References

Agisoft Photoscan User Manual, Retrieved 3/3, 2017, from http://www.agisoft.com/pdf/photoscan-pro_1_3_en.pdf

Aniya, M., J., Naruse, R. (1986). Mapping Structure and Morphology of Soler Glacier, in Northern Patagonia, Chile, Using Near-vertical, Aerial Photographs, Taken with a Non-metric, 6×6 CM-format Camera, *Annals of Glaciology 8*, 1986, Retrieved 7/18, 2017, from https://services.lib.mtu.edu:4630/core/services/aop-cambridge-core/content/view/625304979CB13381AF0BAF9EE82ADC3B/S0260305500001038a.pdf/mapping_structure_and_morphology_of_soler_glacier_in_northern_patagonia_chile_using_nearvertical_aerial_photographs_taken_with_a_nonmetric_6_x_6_cmformat_camera.pdf

Barrile, V., Bilotta, G., Lamari, D., Meduri, G. M. (2015). Comparison between techniques for generating 3D models of cultural heritage, *Recent Advances in Mechanics, Mechatronics and Civil, Chemical and Industrial Engineering*, 2015, 140-145

Bolognesi, M., Furini, A., Russo, V., Pellegrinelli, A., Russo, P. (2014). Accuracy of Cultural Heritage 3D Models by RPAS and Terrestrial Photogrammetry, *ISPRS - International Archives of the Photogrammetry, Remote Sensing and Spatial Information Sciences*, Volume XL-5, 2014, 113-119.

Brown, D.C. (1971). Close range camera calibration, *Photogrammetric Engineering*, XXXVII(8), 855–866.

Busby, J. (2016), 3D Scanning Reflective Objects With Photogrammetry, Accessed 3/5, 2017, from http://www.3dscanstore.com/index.php?route=journal2/blog/post&journal_blog_post_id=19.

Caroti, G., Martinez-Espejo Zaragoza, I., Piemonte, A. (2015). Accuracy Assessment in Structure from Motion 3D Reconstruction from UAV-born

Images: the Influence of the Data Processing Methods, *ISPRS - International Archives of the Photogrammetry, Remote Sensing and Spatial Information Sciences*, Volume XL-1/W4, 2015, 103-109.

Deng, F., Kang, J., Li, P., Wan, F. (2015). Automatic true orthophoto generation based on three-dimensional building model using multiview urban aerial images, *Journal of Applied Remote Sensing*, Vol. 9, 2015, Retrieved 3/15, 2017, from http://remotesensing.spiedigitallibrary.org/article.aspx?articleid=2203881

Fonstad, M.A., Dietrich, J.T., Courville, B.C., Jensen, J.L., Carbonneau, P.E. (2012). Topographic Structure from Motion: a New Development in Photogrammetric measurement, *Earth Surface Process and Landforms* 38, 421-430.

Fraser, C.S. (1997). Digital Camera Self-calibration, *ISPRS Journal of Photogrammetry & Remote Sensing* 52 (1997) 149-159.

Griggs, B. (2014). This May Be the Oldest Surviving Photo of a Human, Accessed 7/2, 2017, from http://www.cnn.com/2014/11/06/living/oldest-photograph-human-daguerre/index.html

Kraus, K., (2004). *Photogrammetry: Geometry from Images and Laser Scans, Second Edition*, Walter de Gruyter GmbH & Co. KG, 10785 Berlin, Germany, 2007, Print.

Mansurov, N. (2017). Understanding Aperture – A Beginner's Guide, Accessed 6/29, 2017, from https://photographylife.com/what-is-aperture-in-photography

Schaich, M. (2013). Combined 3D Scanning and Photogrammetry Surveys with 3D Database Support for Archaeology & Cultural Heritage. A Practice Report on ArcTron´s Information System aSPECT$^{3D.}$, *Photogrammetric Week 13*, 2013, 233-246.

Westoby, M.J., Brasington, J., Glasser, N.F., Hambrey, M.J., Reynolds, J.M. (2012). 'Structure-from-Motion' photogrammetry: A low-cost, effective tool for geoscience applications, *Geomorphology* 179 (2012) 300–314.

Wolf, P.R., Dewitt, B.A., Wilkinson, B.E. (2014). *Elements of Photogrammetry with Applications in GIS, Forth Edition*, McGraw-Hill Education, 2014, Print.

Appendix: MATLAB codes

Code for calculation of standard deviation and RMSE of the plane

```
clear; clc; close all;

point=pcread('E:\SU3600\105-2.ply');
t=pcread('E:\Papers\Report\105_14.ply');

[I,J]=size(t.Location);

figure(1)
pcshow(t);

[n,V,p]=affine_fit(t.Location);

%n(1)=a;n(2)=b;n(3)=c
d=p(1)*n(1)+p(2)*n(2)+p(3)*n(3);

dist=[];
for i=1:I

dist1=(n(1)*t.Location(i,1)+n(2)*t.Location(i,2)+n(3)*t.Locati
on(i,3)-d)/sqrt(n(1)^2+n(2)^2+n(3)^2);
    dist=[dist;dist1];
end
s=0;
for i=1:I
    s=s+dist(i)^2;
end

std=sqrt(s/I);

W=find(point.Location(:,1)>=t.XLimits(1)&point.Location(:,1)<=
```

```
t.XLimits(2)&point.Location(:,2)>=t.YLimits(1)&point.Location(
:,2)<=t.YLimits(2)&point.Location(:,3)>=t.ZLimits(1)&point.Loc
ation(:,3)<=t.ZLimits(2));
pointsub=point.Location(W,1:3);

[n1,V1,p1]=affine_fit(pointsub);

d1=p1(1)*n1(1)+p1(2)*n1(2)+p1(3)*n1(3);

[I1,J1]=size(pointsub);
dist0=[];
for i=1:I1

dist2=(n1(1)*pointsub(i,1)+n1(2)*pointsub(i,2)+n1(3)*pointsub(
i,3)-d1)/sqrt(n1(1)^2+n1(2)^2+n1(3)^2);
    dist0=[dist0;dist2];
end
s1=0;
for i=1:I1
    s1=s1+dist0(i)^2;
end

std1=sqrt(s1/I1);
figure(2);
plot3(pointsub(:,1),pointsub(:,2),pointsub(:,3),'.')
```

Code for calculation of standard deviation and RMSE of different colors

```
clear; clc; close all;

point=pcread('E:\SU3600\105-20.ply');
t=pcread('E:\Papers\Report\scan\w1.ply');
t1=pcread('E:\Papers\Report\scan\w2.ply');
t2=pcread('E:\Papers\Report\scan\w3.ply');
```

```
t3=pcread('E:\Papers\Report\scan\w4.ply');
t4=pcread('E:\Papers\Report\scan\w5.ply');
t5=pcread('E:\Papers\Report\scan\w6.ply');
t6=pcread('E:\Papers\Report\scan\w7.ply');
t7=pcread('E:\Papers\Report\scan\w8.ply');
t8=pcread('E:\Papers\Report\scan\w9.ply');
t9=pcread('E:\Papers\Report\scan\w10.ply');

[I,J]=size(t.Location);

figure(1)
pcshow(t);

[n,V,p]=affine_fit(t.Location);

%n(1)=a;n(2)=b;n(3)=c
d=p(1)*n(1)+p(2)*n(2)+p(3)*n(3);

dist=[];
for i=1:I

dist1=(n(1)*t.Location(i,1)+n(2)*t.Location(i,2)+n(3)*t.Locati
on(i,3)-d)/sqrt(n(1)^2+n(2)^2+n(3)^2);
    dist=[dist;dist1];
end
s=0;
for i=1:I
    s=s+dist(i)^2;
end

std=sqrt(s/I);

W=find(point.Location(:,1)>=t.XLimits(1)&point.Location(:,1)<=
t.XLimits(2)&point.Location(:,2)>=t.YLimits(1)&point.Location(
```

```
:,2)<=t.YLimits(2)&point.Location(:,3)>=t.ZLimits(1)&point.Loc
ation(:,3)<=t.ZLimits(2));
W1=find(point.Location(:,1)>=t1.XLimits(1)&point.Location(:,1)
<=t1.XLimits(2)&point.Location(:,2)>=t1.YLimits(1)&point.Locat
ion(:,2)<=t1.YLimits(2)&point.Location(:,3)>=t1.ZLimits(1)&poi
nt.Location(:,3)<=t1.ZLimits(2));
W2=find(point.Location(:,1)>=t2.XLimits(1)&point.Location(:,1)
<=t2.XLimits(2)&point.Location(:,2)>=t2.YLimits(1)&point.Locat
ion(:,2)<=t2.YLimits(2)&point.Location(:,3)>=t2.ZLimits(1)&poi
nt.Location(:,3)<=t2.ZLimits(2));
W3=find(point.Location(:,1)>=t3.XLimits(1)&point.Location(:,1)
<=t3.XLimits(2)&point.Location(:,2)>=t3.YLimits(1)&point.Locat
ion(:,2)<=t3.YLimits(2)&point.Location(:,3)>=t3.ZLimits(1)&poi
nt.Location(:,3)<=t3.ZLimits(2));
W4=find(point.Location(:,1)>=t4.XLimits(1)&point.Location(:,1)
<=t4.XLimits(2)&point.Location(:,2)>=t4.YLimits(1)&point.Locat
ion(:,2)<=t4.YLimits(2)&point.Location(:,3)>=t4.ZLimits(1)&poi
nt.Location(:,3)<=t4.ZLimits(2));
W5=find(point.Location(:,1)>=t5.XLimits(1)&point.Location(:,1)
<=t5.XLimits(2)&point.Location(:,2)>=t5.YLimits(1)&point.Locat
ion(:,2)<=t5.YLimits(2)&point.Location(:,3)>=t5.ZLimits(1)&poi
nt.Location(:,3)<=t5.ZLimits(2));
W6=find(point.Location(:,1)>=t6.XLimits(1)&point.Location(:,1)
<=t6.XLimits(2)&point.Location(:,2)>=t6.YLimits(1)&point.Locat
ion(:,2)<=t6.YLimits(2)&point.Location(:,3)>=t6.ZLimits(1)&poi
nt.Location(:,3)<=t6.ZLimits(2));
W7=find(point.Location(:,1)>=t7.XLimits(1)&point.Location(:,1)
<=t7.XLimits(2)&point.Location(:,2)>=t7.YLimits(1)&point.Locat
ion(:,2)<=t7.YLimits(2)&point.Location(:,3)>=t7.ZLimits(1)&poi
nt.Location(:,3)<=t7.ZLimits(2));
W8=find(point.Location(:,1)>=t8.XLimits(1)&point.Location(:,1)
<=t8.XLimits(2)&point.Location(:,2)>=t8.YLimits(1)&point.Locat
ion(:,2)<=t8.YLimits(2)&point.Location(:,3)>=t8.ZLimits(1)&poi
nt.Location(:,3)<=t8.ZLimits(2));
```

```
W9=find(point.Location(:,1)>=t9.XLimits(1)&point.Location(:,1)
<=t9.XLimits(2)&point.Location(:,2)>=t9.YLimits(1)&point.Locat
ion(:,2)<=t9.YLimits(2)&point.Location(:,3)>=t9.ZLimits(1)&poi
nt.Location(:,3)<=t9.ZLimits(2));

BLK=[W;W1;W2;W3;W4;W5;W6;W7;W8;W9];
pointsub=point.Location(BLK,1:3);

[n1,V1,p1]=affine_fit(pointsub);

d1=p1(1)*n1(1)+p1(2)*n1(2)+p1(3)*n1(3);

[I1,J1]=size(pointsub);
dist0=[];
for i=1:I1

dist2=(n1(1)*pointsub(i,1)+n1(2)*pointsub(i,2)+n1(3)*pointsub(
i,3)-d1)/sqrt(n1(1)^2+n1(2)^2+n1(3)^2);
    dist0=[dist0;dist2];
end
s1=0;
for i=1:I1
    s1=s1+dist0(i)^2;
end

std1=sqrt(s1/I1);
figure(2);
plot3(pointsub(:,1),pointsub(:,2),pointsub(:,3),'.');
```

Code for the graphs

```
clear;clc;close all;

No=[5814288;
```

```
    1487968;
    698168;
    394093;
    250087;
    184325;
    135518;
    101224;
    83578;
    67684];
X=[2;
   4;
   6;
   8;
   10;
   12;
   14;
   16;
   18;
   20];

figure(1)
plot(X,No,'r-*');

S=csvread('E:\Papers\Report\STDs.csv');

figure(2)
plot(X,flipud(S(:,1)),'r-d',...
    'LineWidth',2,...
    'MarkerSize',10,...
    'MarkerFaceColor',[1,0.5,0.5]);
hold on;
plot(X,flipud(S(:,2)),'g--o',...
    'LineWidth',2,...
    'MarkerSize',10,...
```

```
    'MarkerFaceColor',[0.5,1,0.5]);
plot(X,flipud(S(:,3)),'b:s',...
    'LineWidth',2,...
    'MarkerSize',10,...
    'MarkerFaceColor',[0.5,0.5,1]);
hold off;
legend('Whole','Black','White','Location','northwest');
title('Standard Deviation');
xlabel('Distances/m');
ylabel('STD/m');

R=csvread('E:\Papers\Report\RMSE_1.csv');

figure(3)
plot(X,flipud(R(:,1)),'r-d',...
    'LineWidth',2,...
    'MarkerSize',10,...
    'MarkerFaceColor',[1,0.5,0.5]);
hold on;
plot(X,flipud(R(:,2)),'g--o',...
    'LineWidth',2,...
    'MarkerSize',10,...
    'MarkerFaceColor',[0.5,1,0.5]);
plot(X,flipud(R(:,3)),'b:s',...
    'LineWidth',2,...
    'MarkerSize',10,...
    'MarkerFaceColor',[0.5,0.5,1]);
hold off;
legend('Whole','Black','White','Location','northwest');
title('Root Mean Square Error');
xlabel('Distances/m');
ylabel('RMSE/m');

figure(4)
```

```
plot(X,flipud(S(:,1)),'r-d',...
    'LineWidth',2,...
    'MarkerSize',10,...
    'MarkerFaceColor',[1,0.5,0.5]);
hold on;
plot(X,flipud(R(:,1)),'g--o',...
    'LineWidth',2,...
    'MarkerSize',10,...
    'MarkerFaceColor',[0.5,1,0.5]);
hold off;
legend('STD','RMSE','Location','northwest');
title('Standard Deviation and Root Mean Square Error');
xlabel('Distances/m');
ylabel('STD and RMSE/m');
```